Nanoscale

Accepted Manuscript

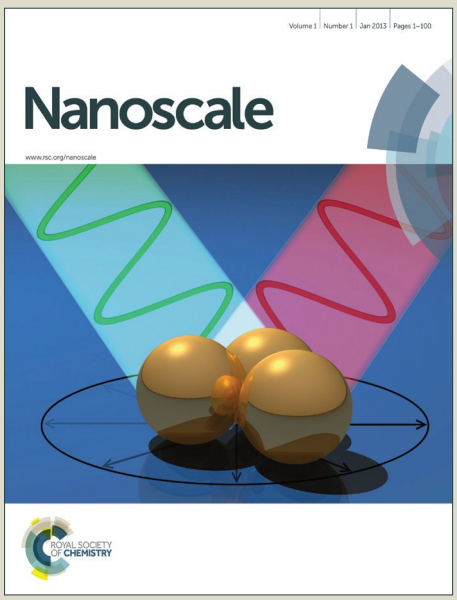

ROYAL SOCIETY OF CHEMISTRY

www.rsc.org/nanoscale

Cite this: DOI: 10.1039/c0xx00000x

www.rsc.org/xxxxxx

ARTICLE TYPE

Tunable Ferromagnetic Ordering in MoS_2 nanosheets with Fluorine Adsorption

Daqiang Gao, Shoupeng Shi, Kun Tao, Baorui Xia and Desheng Xue*

Received (in XXX, XXX) Xth XXXXXXXXX 20XX, Accepted Xth XXXXXXXXX 20XX

DOI: 10.1039/b000000x

Two-dimensional ferromagnetic ultrathin nanosheets hold great promise for next generation electronics and spintronics. Here, intrinsic ferromagnetism were achieved through a new effective strategy by fluorine adsorption on MoS_2 nanosheets, where the fluorinated MoS_2 nanosheets exhibit stable ferromagnetic hysteresis at room temperature with saturation magnetization of 0.06 emu/g and the magnetoresistance of 4.1 %. The observed ferromagnetism can be tuned by changing the concentration of the adatom. On the basis of first-principle calculations, it is shown that not only fluorine absorbed MoS_2 monolayer favours spontaneous spin polarization and local moment formation, but also that the spin moments can exhibit long range magnetic ordering. This work paves a new pathway to engineer the magnetic properties of the two-dimensional nano-materials.

Two-dimensional (2D) crystals of transition metal dichalcogenides (TMDs) have received significant interest due to their potential in a wide range of novel applications as well as in basic research.[1–3] As the member of the TMDs family, molybdenum disulfide (MoS_2) isolated in the single-layer form was first to attract attention, demonstrating high on/off current ratio and low off-state current.[4] Recently, integrated circuits based on single-layer MoS_2, bilayer MoS_2, signal amplifiers, and nonvolatile memory cells were also demonstrated.[5-7] What's more, the presence of a direct band gap in MoS_2 due to the dimensional confinement makes it interesting for applications in optoelectronics.[8-10]

In addition, studies on the magnetic response of MoS_2 were also proposed recent, proving its potential application in spintronics and nanoelectronic devices. Many theoretical studies suggested that, although bulk MoS_2 is a diamagnetic material like graphite, the MoS_2 becomes ferromagnetic when MoS_2 nanoribbons are formed with zigzag edges, or defects are induced.[11,12] Experimentally, ferromagnetism was obtained in freestanding nanosheets,[13] the vertically aligned nanosheets,[14] and in the bulk MoS_2 irradiated by proton,[15] where the existence of ferromagnetism was partly attribute to the presence of zigzag edges or defects states at the grain boundaries. However, for its use in nanoelectronics, the magnetic coupling modulated by the edges and defects states in MoS_2 nanosheets is always somewhat rough as compared to the ideal requirement (stable and precision magnetic spin ordering) and, thus, is inconvenient to control in the actual application, which hampers the development of this material in nanoelectronic devices.[16]

Previous studies have found that the absorption of nonmetal element on the surface of low-dimensional systems can induce local magnetic moment.[17,18] Compared with the magnetic moment from *d* or *f* electrons of transition-metal or rare-earth atoms, the magnetism based on the *sp* states of nonmetal element has some obvious advantage, such as stronger long-range exchange coupling interactions and no clustering of magnetic ions. Fluorination was confirmed to be the most effective route to introduce localized spins in graphene and it has been reported that the fluorination can induce tunable magnetism in the BN nanotubes and the nanosheets.[19,20] Recently, the published studies on the possible magnetic properties of fluorinated TMDs are also performed in theoretical nature. For example, He *et al*. investigated the adsorption of nonmetal atoms on pristine MoS_2 and found that H, B, C, N and F atoms can induce local magnetic moments.[21] Yue *et al.* study the magnetic and electronic properties of MoS_2 sheets with substitution of H, B, C, O, N and F atoms with sulfur defects (V_S). Calculated binding energies show that all the substitutional atoms are strongly bound to V_S defects, resulting in different magnetic behaviors.[22] These anticipate results opening a new way to modify the magnetic properties of the monolayer MoS_2. However, examining the magnetic properties of non-metal atoms absorbed MoS_2 has not been realized experimentally. Therefore, it is of crucial importance to develop a feasible method for synthesizing them and explore the corresponding magnetic properties.

In this paper, we reported the preparation and corresponding magnetic properties of the fluorinated MoS_2 (F-MoS_2) nanosheets. First-principles calculations results demonstrate that F atom can chemically absorb on MoS_2 monolayer favouring the top of S atom, where total magnetic moment of 1.0 μ_B was found in F-absorbed MoS_2 monolayer. Magnetic measurements results indicate that the enhancement of the room temperature ferromagnetism was observed for F-MoS_2 nanosheets compared to the primitive nanosheets, which

material is quite promising for applications in spintronic devices.

Results and discussions

F-MoS_2 nanosheets were prepared by a two-step method as shown in Fig. 1a. In brief, ultrathin MoS_2 nanosheets were first gotten by exfoliating the bulk form in N,N-Dimethylformamide (DMF, 100 mL) solution as our previous report. [13] Then, 1.0 g of the exfoliated MoS_2 nanosheets and 2.0 g ammonium fluoride (NH_4F) were further ground into a homogeneous form with the deionized water and transferred in a Teflon-lined stainless steel autoclave, which system was heated at 180 ℃ for 24 h and then cooled down to room temperature. The autoclave container was taken out and the product was centrifuged and washed with ethanol and deionized water repeatedly. Finally, the as-obtained sample was dried in a vacuum oven for 24 h. Subsequently, systematical characterizations were performed to verify that the finally products were in ultrathin nanosheet structure. Transmission electron microscope (TEM, TecnaiTM G2 F30, FEI, USA) image of F-MoS_2 nanosheets shown in Fig. 1b revealed that the lateral diameters of the nanosheets are ~200 nm. Results indicate that the colloidal dispersions of the F-MoS_2 nanosheets are highly stable over a period of several days and display a typical Tyndall effect, reasonably indicating the formation of freestanding and homogeneous 2D ultrathin sheets (inset in Fig. 1b). The further high resolution TEM results for the selected regions of one nanosheet is shown in Fig. 1c, indicating that the nanosheets is well crystallographic. The thickness of the products was measured by the Atomic force microscopy (AFM Dimension 3100 with Nanoscope IIIa controller, Veeco, CA, USA). As can be seen from Fig. 1d, the thicknesses of ultrathin nanosheets are ranging from 2.9 nm to 3.4 nm, which indicates the ultrathin nanosheets are composed of 3~5 atomic monolayers.

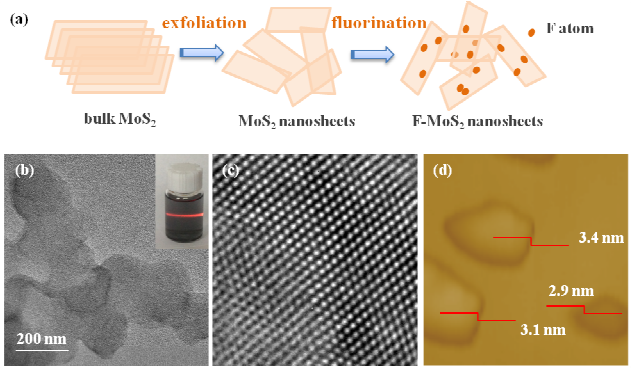

Fig. 1. (a) Schematic illustration for the synthesize of fluorination-MoS_2 nanosheets. (b) TEM and the corresponding colloidal DMF dispersion displaying the Tyndall effect. (c) HRTEM (d) AFM image and the corresponding height profile for the fluorination-MoS_2 nanosheets.

Typical X-ray diffraction (XRD, X' Pert PRO PHILIPS with Cu Kα radiation) spectrum of the F-MoS_2 nanosheets is shown in Fig. 2a, it is possible to assign the reflection peaks to the family lattices planes of hexagonal MoS_2 (JCPDS Card No.77-1716). Result indicates there is no other new phase introducing for the fluorination progress. What's more, the bonding characteristics and the composition of the exfoliated MoS_2 samples were captured by X-ray photoelectron spectroscopy (XPS, Kratos Axis Ultra). Besides element of C, the wide XPS spectra of the F-MoS_2 sample show only signals arising from elements Mo, S and F. The peaks, corresponding to the S $2p_{1/2}$ and S $2p_{3/2}$ orbital of divalent sulfide ions (S^{2-}), are observed at 163.3 and 162.0 eV shown in Fig. 2b. The Mo 3*d* XPS spectrum of F-MoS_2 nanosheets, reported in Fig. 2c shows two strong peaks at 229.3 and 232.5 eV, respectively, attributed to the doublet Mo $3d_{5/2}$ and Mo $3d_{3/2}$. Besides, the peak at the binding energy of 686.9 eV attributes to the F 1*s* specture. All these results are consistent with the reported values.[23] Elemental mapping results shown in Fig. 2 f~i also give the information that the samples contain element Mo, S and F, where the elemental distribution are uniformly.

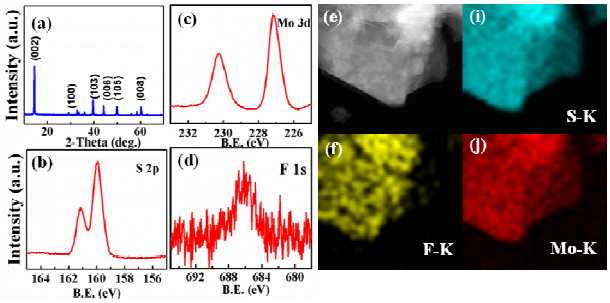

Fig. 2. (a) XRD (b)~(d) XPS results, and (e)~(j) TEM image and the elemental mapping for the fluorination-MoS_2 nanosheets.

The magnetic properties of the F-MoS_2 nanosheets were studied by using a superconducting quantum interferometer device (SQUID) magnetometer from Quantum Design. Fig. 3a shows the magnetization curves (*M-H*) of the F-MoS_2 nanosheets measured at different temperatures (10~300 K) and the magnetization curve for the exfoliated MoS_2 nanosheets was also given to compared, where the diamagnetic background have been subtracted (the primitive curves are shown in Fig.S1†). It can be seen that the exfoliated MoS_2 nanosheets show the saturation magnetization (M_s) of 0.001 emu/g at 300 K, which is corresponding to our previous result, where the ferromagnetism is considered to be related to the edge states.[13] However, it is interesting that the sample's M_s shows the great enhancement after fluorination. As shown in Fig. 3a, the F-MoS_2 nanosheets have the M_s of 0.07 and 0.06 emu/g at 10 and 300 K, respectively. The magnetic hysteresis loops measured in the low field range are plotted in Fig. S2†. Obviously, ferromagnetic behaviour of the F-MoS_2 is robust at this temperature range with the remanent magnetic moment (M_r) and coercivity (H_c) decreases with the increase of temperature. In addition, temperature dependent magnetization (*M-T*) curves of the F-MoS_2 nanosheets presented in Fig. 3b provide another evidence to prove the sample is intrinsically room temperature ferromagnetism. Obviously, zero field cooling (ZFC) and field cooling (FC) curves showed distinct difference in wide temperature range from 10 up to 300 K, revealing Curie temperature is higher than 300 K. Most importantly, there is no block temperature appearance in ZFC curve, which clearly reveals that there are no ferromagnetic clusters in our sample and provides evidence

for ferromagnetism in the samples.[24] Besides, it can be seen that there is a magnetic moments change at about 120 K in the FC curve. Such magnetic anomaly was found when antiferromagnetic (AFM) correlations competed with ferromagnetic (FM) interactions. This result was similar to that obtained for graphene,[25,26]somewhat like spin glass behavior in frustrated system. Though the origin remained unclear, a coexistence of ferromagnetism and antiferromagnetism was well accepted for a biparticle system.[27] Magnetic measurement results indicate that the raw materials (h-MoS_2 powder and NH_4F) show diamagnetism only (see Fig.S3†). Thus, we conclude that the enhanced ferromagnetism observed in the F-MoS_2 nanosheets is mainly induced by fluorination. Of note, the ferromagnetic impurities such as Fe, Co, Ni could also be excluded by inductively coupled plasma (ICP) results, which contents are all below 10 ppm. Therefore, all above analyses confirmed that the room temperature ferromagnetism in F-MoS_2 nanosheets is inherent nature.[28,29]

By using the SQUID and vibrating sample magnetometer equipped with a high temperature chamber (VSM, VSM Model EV9, MicroSense, LLC), we could get the information of M_S dependence on temperature for the F-MoS_2 nanosheets. As shown in Fig. 3c, the dates can be well fitted by the following equation which is common for a ferromagnetic material: [30,31] $M(T)=A(1-T/T_C)^{\beta}$, where A is a coefficient related to the spontaneous magnetization, T_C is theferromagnetic Curie temperature, and β is the critical exponent. The best fitting curve ($T<T_C$) is shown by red curve, where the fitted sample's Cure temperature is about 845 K. Such high T_C ferromagnetism in few-layer F-MoS_2 nanosheets makes them promising candidates for application in spintronic devices.[32,33] Besides. we also studied the affect of amount of fluoride on the magnetic properties of the F-MoS_2 nanosheets.

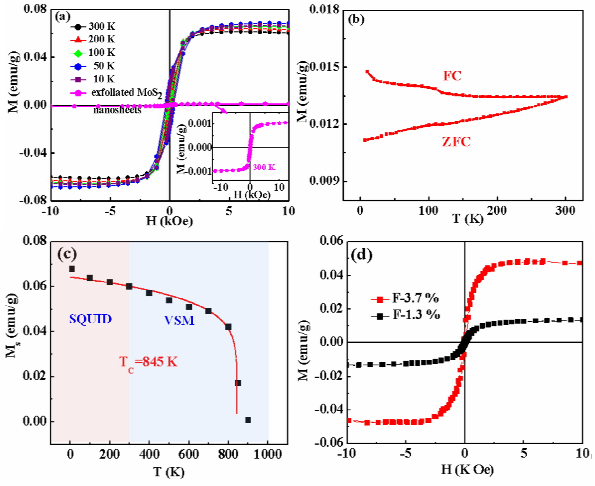

Fig. 3. (a) Magnetization curves (M-H) of the fluorination-MoS_2 nanosheets measured at different temperatures (10~300 K), where the diamagnetic background have been subtracted. (b) Temperature dependence of zero field cooling (ZFC) and field cooling (FC) curves of fluorination-MoS_2 nanosheets under the measuring field of 200 Oe. (c) Ms dependence on temperature for the fluorination-MoS_2 nanosheets (10~900 K). (d) M-H curves of fluorination-MoS_2 nanosheets fabricated with different mounts of NH_4F at 300 K.

We changed the quality of NH_4F from 2.0 g to 1.5 g and 0.5 g, respectively, in the experiment progress with the other conditions identical, where the concentration of fluorine atoms were 1.3 %, 3.7 % and 7.0 % with the F^- electron state for the three samples (NH_4F=0.5 g, 1.0 g and 2.0 g), which were gotten by XPS measurement. As can be seen from Fig. 3d that the F-MoS_2 nanosheets show different M_s, indicating that ferromagnetism of the samples can be tuned by changing the concentration of the adsorption atoms.

Above results indicate that the observed larger ferromagnetism in F-MoS_2 nanosheets is mainly induced by introducing the F atom absorbed on the MoS_2 nanosheets. To further understand how fluoride influence the ferromagnetism in MoS_2 nanosheets, the geometries, electronic structures, and magnetic behaviour of F-absorbed MoS_2 monolayers were investigated by using first principles calculations. The studied model consists of a 4×4×1 MoS_2 supercell (including 32 S and 16 Mo atoms) and an adatom (F atom). The distance between two adjacent MoS_2 monolayers is larger than 16 Å to avoid the layer-layer interaction. Calculations results indicate that the most energetically favorable absorbed position is at the top of S atom for the adatom. The spin-polarized calculations within density functional theory formalism were performed using the Vienna *ab* intio simulation package (VASP) with the generalized gradient approximation of Perdew–Burke–Ernzerhof functional.[34] The plane wave basis set with kinetic energy cutoff of 500 eV was employed. The sampling of the Brillouin zone was done using a 5×5×1 Monkhorst–Pack grid. All the structures were fully relaxed until the Hellmann–Feynman force was less than 0.01 eV/Å.[35]

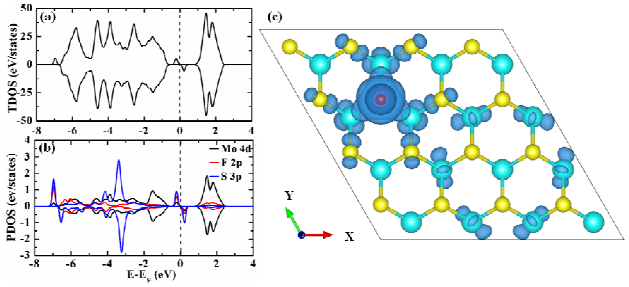

Fig. 4. (a) The TDOS and (b) PDOS of the F-absorbed MoS_2 monolayers. The black, red, and blue lines represent the nearest Mo atom, the adatom, and the nearest S atom, respectively. (b) The spin resolved charge density isofurface (0.001 $Å^{-3}$) of the F-absorbed MoS_2 monolayers. Mo atoms are indicated by blue balls, S atoms by yellow balls and F atoms by red balls, respectively.

As shown in Fig. 4a, a significant asymmetry between the spin-up state and spin-down state in the density of states (DOS) near the Fermi level suggests the intrinsic ferromagnetism of F-absorbed MoS_2 monolayer. As well known, the value of the Curie temperature depends on the exchange stiffness and the DOS at the Fermi level. The calculated DOS display obvious spin splitting at the conduction band and valence band means the relative high Curie temperature in this configuration, which is identical with our experimental results. The total magnetic moments of this electronic structure is about 1.0 μ_B. The spin-resolved

DOS projected on the 4*d* orbital of the nearest Mo atom, *p* orbitals of the adatom and the nearest S atom are also presented in the Fig. 4b. All of them show significant asymmetry between the spin-up state and spin-down state near the Fermi level, illustrating both of them contribute the magnetic moment to the total magnetic moments. Obviously, the PDOS results clearly uncovers that the 2*p* orbital of the adatom are localized, spin-polarized, and consequently induces polarizations of S 3*p* and Mo 4*d* electrons nearby the adatoms. Near the Fermi energy, the spin-up states are full occupied and the spin-down states are unoccupied or partially occupied, which is the origin of magnetic moment for the F-adsorbed MoS_2 monolayer. These results are consistent with the spin resolved charge density distribution of the F-absorbed MoS_2 monolayers as shown in Fig. 4c. It is worth noting that the overlaps between F 2*p* states and 3*s* states of the second-nearest S, 4*d* states of the third-nearest Mo atoms are still evident, which corresponds to the large spatial extension of spin density of F-MoS_2 monolayer.

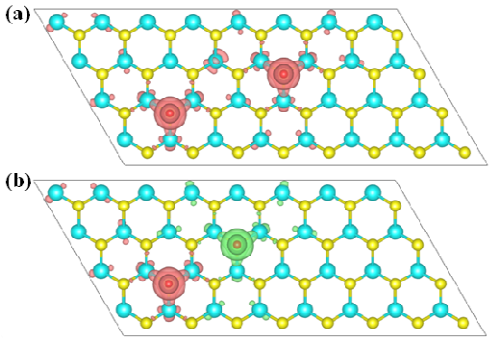

Fig. 5. Spatial distribution of the spin-polarization density of the MoS_2 monolayers with two F atoms absorbed. (a) ferromagnetism coupling, (b) antiferromagnetism coupling . The unit is $Å^{-3}$, Mo atoms are indicated by blue balls, S atoms by yellow balls and F atoms by red balls, respectively.

To further study the magnetic coupling between the fluorination induced local magnetic moments, we adopted large-size supercells containing 32 primitive cells (denoted as 8×4×1) and two F ions, which correspond to the fluorination rate of 1/16 in a MoS_2 monolayer. Starting from different initial spin arrangement, self-consistent calculations lead to two types of magnetic orderings. One has the local magnetic moments aligned in a "FM" way. Another has the local magnetic moments aligned in an "AFM" way. [36,37] Calculation results indicate that two stable magnetic structures were obtained: one was FM (E_{AFM}–E_{FM}= 0.32 meV), the other was AFM (E_{AFM}–E_{FM}= −0.48 meV). It can be seen from Fig. 5a that most of the spin polarized states localized around the F dopants and leaded to the formation of local magnetic moment while the long range magnetic coupling was mediated between the two moments. However, as the distance between two F dopants decreased, the system would be more stable in the AFM phase, due to the broaden of the dopant band equal to spin split, caused by the larger degree of overlap between the unpaired electrons (Fig. 5b). These results are similar to the reports of C doped BN and defective C_{60} systerms.[36,38] To sum up, above calculations results indicate that the spin moments induced by topological fluorine adsorption on MoS_2 nanosheets can be (anti)ferromagnetically coupled to exhibit long rang magnetic ordering, which is corresponding to the experimental results.

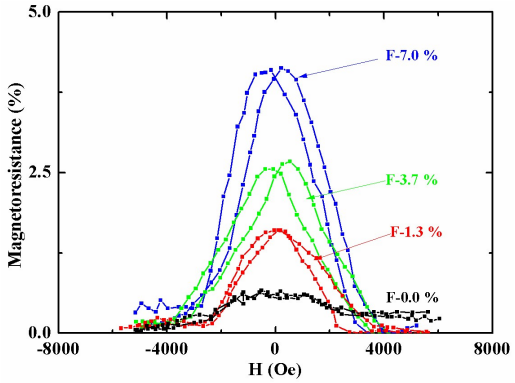

Fig. 6. MR curves of the fluorination-MoS_2 nanosheets measured at room temperature.

In order to check the intrinsic nature of the ferromagnetism in F-MoS_2 nanosheets and its possible spintronics applications, we measured magnetoresistance (MR) of F-MoS_2 nanosheets by two-terminal method, where the F-MoS_2 nanosheets were pressed into a 5 mm-diameter piece. The MR results for the samples with different F contents are shown in Fig. 6 in the field range of -8000 Oe < H < 8000 Oe, where the MR value is defined as $[R(H)-R(0)]/R(0)$ and $R(0)$ is the resistance at zero field. It can be seen that all the samples show hysteresis negative MR curves, where the sample with the F content of 7.0 % shows the max MR value of 4.1 %. Similar negative hysteresis MR has been observed in reduced graphene oxide and VS_2 nanosheets, which is a clear indication of the intrinsic nature of the observed ferromagnetism.[39,40]

In addition, we have quantitatively analyzed the magnetization signal to get the magnetic moment per absorb F atom. Results indicate that the F concentration for sample F-MoS_2-2.0 is about 7.0 %. Therefore, with a F/Mo+S+F ratio of 7%, the number of F dopants per unit mass, was given by $N_C = (N_A/M_R)\times 7\% = 2.63\times 10^{20}$ dopants/g,[36] where M_R was the relative molecular weight of MoS_2 (160.06) and N_A was the Avogadro's constant of 6.02×10^{23}. The value of the M_s for the F-MoS_2 nanosheets was 0.07 emu/g as shown in Figure 3a, and, thus, the magnetic moment per absorbed F was given by $\mu_C = M_s/N_C = 1.16\times 10^{-22}$ emu $= 1.25\times 10^{-2}\,\mu_B$. Comparing with our theoretical value of 1.0 μ_B per F dopant, only 1/8 F dopants seemed to contribute to the ferromagnetism in experiment. Noting that we used a MoS_2 monolayer model in these calculations, for the synthesized F-MoS_2 nanosheets which contain multi-layers, the fluorination rate will be lower than this model. In addition, the reason may be that some absorbed F atoms formed islands on the surfaces of MoS_2 nanosheets. Apart from these, some AFM coupling also make the total magnetic moment from these two F dopants to be zero. Therefore, only those F dopants that had no counterparts on the vicinal site sublattice would contribute to total magnetic moment to F-MoS_2

nanosheet in our case. However, to what extent each factor will play a role is still a question and our work is on the way.

Conclusions

In summary, we have demonstrated that involving of F atoms absorbed on MoS_2 nanosheets can induce intrinsic ferromagnetism, which is verified by both magnetic characterizations and theoretical calculations. The saturation magnetization of F-MoS_2 nanosheets at room temperature was as high as 0.06 emu/g, which is larger than that of the exfoliated MoS_2 nanosheets caused by defects and edge state. What's more, hysteresis negative MR curve can be observed for all the samples, revealing its possible spintronics applications. This finding broaden our horizon and it is anticipate that introduction of non-magnetic absorbed strategy could be an effective way for engineering the intrinsic magnetic properties of 2D nanomaterials.

Acknowledgements

This work is supported by National Basic Research Program of China (Grant No. 2012CB933101), the National Natural Science Fundation of China (Grant No. 51371093, 51202101, 11474137, 11274146 and 11034004), Program for Changjiang Scholars and Innovative Research Team in University (Grant No. IRT1251) and the Specialized Research Fund for the Doctoral Program of Higher Education (20120211120005).

Notes and references

*Key Laboratory for Magnetism and Magnetic Materials of MOE, Key Laboratory of Special Function Materials and Structure Design, Ministry of Education, Lanzhou University, Lanzhou 730000, P. R. China. Fax: +86 0931 8914160; Tel: +86 0931 8914160; *E-mail: xueds@lzu.edu.cn;*
† Electronic Supplementary Information (ESI) available]. See DOI: 10.1039/b000000x/

1 K. F. Mak, K. He, J. Shan and T. F. Heinz, Nat. Nanotechnol. 7, 494 (2012).
2 Y. Li, H. Wang, L. Xie, Y. Lang, G. Hong and H. Dai, J. Am. Chem. Soc. 133, 7296 (2011).
3 Q. H.Wang, K. Kalantar-Zadeh, A. Kis, J. N. Coleman and M. S.Strano, Nat. Nanotechnol. 7, 699 (2012).
4 B. Radisavljevic, M. B. Whitwick, A. Kis, ACS Nano, 5, 9934 (2011).
5 H. Wang, L. Yu, Y.-H. Lee, Y. Shi, A. Hsu, M. L. Chin, L.-J. Li, M. Dubey, J. Kong and T. Palacios, Nano Lett. 12, 4674 (2012).
6 B. Radisavljevic, M. B. Whitwick, A. Kis, Appl. Phys. Lett. 101, 043103 (2012).
7 S. Bertolazzi, D. Krasnozhon, A. Kis, ACS Nano, 7, 3246 (2013).
8 D. Ovchinnikov, A. Allain, Y. S. Huang, D. Dumcenco, and A. Kis. ACS Nano, 8, 8174 (2014).
9 Z. Jin, S. Shin, D. H. Kwon, S. J. Han and Y. S. Min, Nanoscale, 6, 14453(2014).
10 J. Xia, X. Huang, L. Z. Liu, M. Wang, L. Wang, B. Huang, D. D. Zhu, J. J. Li, C. Z. Gu and X. M. Meng, Nanoscale, 6, 8949 (2014).
11 C. Ataca, H. S¸ ahin, E. Aktu¨rk, and S. Ciraci, J. Phys. Chem. C 115, 3934 (2011).
12 Y. Li, Z. Zhou, S. Zhang, and Z. J. Chen, J. Am. Chem. Soc. 130, 16739 (2008).
13 D. Gao, M. Si, J. Li, J. Zhang, Z. Zhang, Z. Yang, and D. Xue, Nanoscale Res. Lett. 8, 129 (2013).
14 J. Zhang, J. M. Soon, K. P. Loh, J. Yin, J. Ding, M. B. Sullivian, and P. Wu, Nano Lett. 7, 2370 (2007).
15 S. W. Han, Y. H. Hwang, S. H. Kim, W. S.Yun, J. D. Lee, M. G. Park, S. Ryu, J. S. Park, D. H. Yoo, S. P. Yoon, S. C. Hong, K. S. Kim, and Y. S. Park, Phys. Rev. Lett. 110, 247201 (2013).
16 Y. D. Ma, Y. Dai, M. Guo, C. W. Niu, Y. T. Zhu, and B. B. Huang, ACS Nano. 6, 1695(2012).
17 O. V. Yazyev and L. Helm, Phys. Rev. B 75, 125408 (2007).
18 J. Zeng, K. Chen, C. Sun, Phys. Chem. Chem. Phys. 14, 8032 (2012).
19 Q. Feng, N. Tang, F. Liu, Q. Cao, W. Zheng, W. Ren, X. Wan and Y. Du, ACS Nano 7, 6729 (2013).
20 Z. H. Zhang and W. L. Guo, J. Am. Chem. Soc. 131, 6874 (2009).
21 J. He, K. Wu, R. Sa, Q. Li, Y. Wei, Appl. Phys. Lett. 96, 082504 (2010).
22 Q.Yue, S. L. Chang, S. Q. Qin, J. B. Li, Phys. Lett. A 377, 1362 (2013).
23 M. Du, X. L. Li, A. Z. Wang, Y. Z. Wu, X. P. Hao, and M. W. Zhao, Angew. Chem. 126, 3719 (2014).
24 D. Q. Gao, G. J. Yang, J. Zhang, Z. H. Zhu, M. S. Si, and D. S. Xue, Appl. Phys. Lett. 99, 052502 (2011).
25 H. S. S. R. Matte , K. S. Subrahmanyam , C. N. R. Rao , J. Phys. Chem. C , 113 , 9982 (2009) .
26 L. L. Chen, L. W. Guo, Z. L. Li, H. Zhang, J. J. Lin, J. Huang, S. F. Jin , X. L. Chen, Sci. Rep. 3, 0259911 (2013).
27 O. V. Yazyev , Rep. Prog. Phys. 73 , 056501 (2010).
28 X. Chen, G. Li, Y. Su, X. Qiu, L. Li, and Z. Zou, Nanotechnology, 20(11), 115606 (2009).
29 M. Khalid, M. Ziese, A. Setzer, P. Esquinazi, M. Lorenz, H. Hochmuth, M. Grundmann, D. Spemann, T. Butz, G. Brauer, W. Anwand, G. Fischer, W. A. Adeagbo, W. Hergert, and A. Ernst, Phys. Rev. B, 80, 035331 (2009).
30 H. E. Stanley, Introduction to Phase Transitions and Critical Phenomena, Oxford University Press, Oxford, 1987.
31 Z. L. Yang, D. Q. Gao, J. Zhang, Q. Xu, S. P. Shi, K. Tao, and D. S. Xue, Nanoscale, 7, 650 (2015).
32 O. V. Yazyev, M. I. Katsnelson, Phys. Rev. Lett. 100, 047209 (2008).
33 Y. G. Zhou, Z. G. Wang, P. Yang, X. T. Zu, L.Yang, X. Sun, and F. Gao, ACS Nano, 6 (11), 9727 (2012).
34 G. Kresse and J. Hafner, J. Phys.: Condens. Matter 6, 8245 (1994).
35 J. P. Perdew, K. Burke, and M. Ernzerhof, Phys. Rev. Lett. 77, 3865 (1996).
36 C. Zhao, Z. Xu, H. Wang, J. Wei, W. Wang, X. Bai, and E. Wang, Adv. Funct. Mater. 24, 5985 (2014).
37 H. H. Qiu,Z. J. Wang, X. L. Sheng, Physica B, 421, 46 (2013).
38 Y. H. Kim, J. Choi, K. J. Chang, D. Tomanek, Phys. Rev. B, 68, 125420 (2003).
39 S. Qin, X. T. Guo, Y. Q. Cao, Z. H. Ni, Q. Y. Xu, Carbon, 78, 559 (2014).
40 D. Gao, Q. Xue, X. Mao, W. Wang, Q. Xu, D. Xue, J. Mater. Chem. C, 1, 5909 (2013).